PAPER

Quantifying the performance of perovskite retinomorphic sensors

To cite this article: Cinthya Trujillo Herrera and John G Labram 2021 *J. Phys. D: Appl. Phys.* **54** 475110

View the article online for updates and enhancements.

You may also like

- <u>Streamer inception thresholds derived</u> from a statistical electron transport model Raphael Färber and Christian M. Franck
- Vertical strain-induced modification of the electrical and spin properties of monolayer MoSi₂X₄ (X = N. P. As and Sb)
 Shoeib Babaee Touski and Nayereh Ghobadi
- Quantifying the impact of vibrational nonequilibrium in plasma catalysis; insights from a molecular dynamics model of dissociative chemisorption Kristof M Bal and Erik C Neyts



IOP ebooks™

Bringing together innovative digital publishing with leading authors from the global scientific community.

Start exploring the collection-download the first chapter of every title for free.

J. Phys. D: Appl. Phys. 54 (2021) 475110 (9pp)

https://doi.org/10.1088/1361-6463/ac1d10

Quantifying the performance of perovskite retinomorphic sensors

Cinthya Trujillo Herrera and John G Labram*

School of Electrical Engineering and Computer Science, Oregon State University, Corvallis, OR 97331, United States of America

E-mail: john.labram@oregonstate.edu

Received 27 May 2021, revised 27 July 2021 Accepted for publication 12 August 2021 Published 16 September 2021



Abstract

Perovskite retinomorphic sensors (PRSs) produce an output voltage in response to changes in optical intensity, but not to constant illumination. While these devices have been demonstrated experimentally, there does not yet exist a robust quantitative model for their behaviour. In this report, we derive a simple relationship between output voltage and optical power density in response to a step-change in illumination intensity. From this model we derive a parameter Λ , which can serve as a proxy for PRS performance. We outline a simple strategy to extract Λ from device data and demonstrate this technique on two sets of experimental data. We evaluate a maximum $\Lambda = 5.3 \times 10^{-4}$ cm mW^{-1/2}. We approximate that a target value of $\Lambda = 1$ cm mW^{-1/2} would be adequate for most commercial applications and discuss some optimization strategies that could be followed to increase Λ .

Keywords: retinomorphic, sensor, perovskite, capacitor

(Some figures may appear in colour only in the online journal)

1. Introduction

Perovskite retinomorphic sensors (PRSs) are three-terminal circuit elements which produce an output voltage in response to changes in light intensity, but not to constant illumination [1]. This is in contrast to conventional optical sensors, such as those based on photodiodes [2], which output a current which increases with incident light intensity. A range of event-driven sensor strategies exist [3], some of which have been demonstrated in two-dimensional arrays [4, 5], or for potential use in intraocular prosthesis [6]. Because they are designed to be a single circuit element, it is hoped that PRSs could one day enable low cost, high density arrays, analogous to photodiodes. Since they output a signal in response to movement only, PRSs have potential value where rapid identification of moving objects is critical, such as visual tracking [7] or in autonomous vehicles [8]. While these devices hold great promise, only a proof of principle design has so far been demonstrated [1]. There does not yet exist a convention to quantitatively assess and predict behaviour of PRSs; a prerequisite for future commercialization endeavours.

In this report we outline a simple model to quantify the performance of PRSs. We recommend a strategy to characterise these sensors experimentally and evaluate a figure of merit for their performance. This strategy will enable facile comparison between different devices and between different research groups. We identify a single parameter, which we designate Λ , with units of cm $mW^{-1/2}$, which can serve as a proxy for broad PRS device performance, in an analogous manner to power conversion efficiency (PCE) in solar cells [9] or field effect mobility (μ_{FET}) in transistors [10]. As with PCE and μ_{FET} , PRSs with higher values of Λ are anticipated to be more desirable for commercial applications than those with low Λ values. Our approach is demonstrated on two sets of experimental data, based on our original PRS device design [1]. Using this model we identify the theoretical maximum performance of these devices, realistic target values, and strategies to optimize performance.

^{*} Author to whom any correspondence should be addressed.

2. Experimental details

2.1. Perovskite retinomorphic sensor (PRS) fabrication

Highly doped silicon wafers with a 300 nm thermally grown silicon dioxide (SiO₂) dielectric layer were purchased from University Wafer. Wafers were cut into 1.0 cm × 1.5 cm rectangles using a wafer saw then cleaned using acetone, isopropanol, then a UV-ozone cleaner. Lead iodide/methylammonium iodide (PbI₂/CH₃NH₃I)—dimethylformamide (DMF) complex mixture and dimethyl sulfoxide were mixed in a 1:1 molar ratio then dissolved in DMF. Films of methylammonium lead iodide (MAPbI₃) were spin-coated under atmospheric pressure N2 onto cleaned Si/SiO2 substrates. Ether was used as an anti-solvent. The films were annealed at 100 °C for 10 min. Lead iodide/methylammonium iodide (PbI₂/CH₃NH₃I)—DMF complex mixture was purchased from Tokyo Chemical Industry Co., Ltd (TCI). 15 nm gold or aluminium contacts were deposited via thermal evaporation through shadow masks. Devices had an area of roughly 5 mm² in all cases.

2.2. Retinomorphic thin film sensor characterization

All devices were contacted in an ambient-pressure N_2 glovebox at room temperature using an Everbeing C-2 probe station. The devices were connected in series with a conventional resistor (1 M Ω in all cases studied experimentally), which was held outside of the glovebox. A Keithley 2400 source meter was used to apply a constant voltage, $V_{\rm in}$, across both the photosensitive capacitor and the resistor. The voltage dropped across the external resistor ($V_{\rm out}$) was monitored with a Textronix TDS 3032C digital oscilloscope. Illumination was provided with a ThorLabs SOLIS-525C High-Power Green (525 nm) light emitting diode (LED), controlled with a ThorLabs DC2200 LED Controller.

3. Dependence on output voltage on optical power density

A PRS consists of a photosensitive bilayer capacitor, as depicted in figure 1(a), in series with a conventional (photo-insensitive) resistor, as depicted in figure 1(b). While in the future it will be desirable to have these components integrated vertically, for the purposes of this study we consider the PRS as separate, connected, elements. The voltage applied across the structure is defined as $V_{\rm in}$, the voltage dropped across the capacitor is V_C , and the voltage dropped across the resistor is $V_{\rm out}$. We conventionally measure the voltage dropped across the resistor, not the capacitor, hence the designated subscript. The bilayer capacitor is designed to change capacitance under illumination, and therefore a semiconductor that absorbs visible light is required.

If a constant $V_{\rm in}$ is applied across the circuit in figure 1(b), and the illumination conditions are constant, all the applied voltage can be assumed to be dropped across the capacitor, hence $V_C = V_{\rm in}$, and $V_{\rm out} = 0$. If the illumination conditions change, one can expect the charge density in the

semiconductor to change, and hence the capacitance of the structure to change. This is expected to briefly lead to charge flow onto/off the bottom electrode, temporarily giving rise to an increase in $V_{\rm out}$, before the charge density equilibrates, charge flow stops, and $V_{\rm out}$ returns to zero.

To test these devices experimentally we apply illumination using a commercial LED, placed above the sensor. The LED is switched from 0 mW cm⁻² to a constant optical power density P, at a time we define as t=0. It is reasonable to assume the turn-on time of the LED is much less than the RC constant of the circuit in figure 1(b), and we hence approximate the incident power density as a step function, as depicted in figure 1(c). V_{out} is measured as a function of time in response to this optical stimulus, as shown in the example in figure 1(d). We employ green (peak emission 525 nm) light here to ensure that we generate free charges in the semiconductor [11], while avoiding any potential issues with UV-induced degradation of the material [12].

The maximum voltage can be approximated directly from this data as $V_{\rm max}$. This is in contrast to our previous study [1] where $V_{\rm out}$ was calculated as a function of time, fitted to relevant parameters, and $V_{\rm max}$ would be extracted from the fit. While an element of subjectivity exists in approximating $V_{\rm max}$ in this way, our analysis relies on fitting data as a function of P and hence involves averaging multiple points.

As with our previous report [1], the level of noise is substantial relative to V_{max} in the devices studied here. While sources of noise will be critical considerations for device integration and readout strategies in the future, we here attribute the noise on V_{out} to noise on V_{in} , provided by the voltage source meter, and induced noise on the coaxial cables connecting the senor and source meter to the oscilloscope. While we still see a resolvable signal, and can carry out our analysis, reducing the noise will be important for more accurate parameterization of these sensors. We anticipate the signal-to-noise ratio (S/N)to be an important parameter for these devices, and expect it to be influenced by similar parameters to more conventional semiconductor devices [13]. While a detailed assessment of noise is better suited to a separate study, we recommend parameterizing it by evaluating V_{max} and dividing it by the rootmean-square of the voltage before the application of the incident light (e.g. for t < 0).

Figure 1(e) shows how $V_{\rm max}$ changes as a function of P for three example devices. The points are the mean $V_{\rm max}$ of the three equivalent devices, and the error bars are the standard deviation between devices. When grown via spin coating, polycrystalline films of MAPbI₃ are known [14] to exhibit significant variability in electronic properties between equivalently prepared samples, which is likely to be a large contributing factor to the sample-to-sample variation we observe. Additionally, these test devices are contacted using probe needles, meaning the electrical contact (and hence contact resistance) may not be equivalent for every measurement.

In our design, we employ highly doped silicon as the bottom electrode and 300 nm of thermally grown SiO₂ as the insulator. SiO₂ is chosen because it is highly resistive, and stable under illumination [13]. For the semiconductor we employ the prototypical metal halide perovskite compound: MAPbI₃

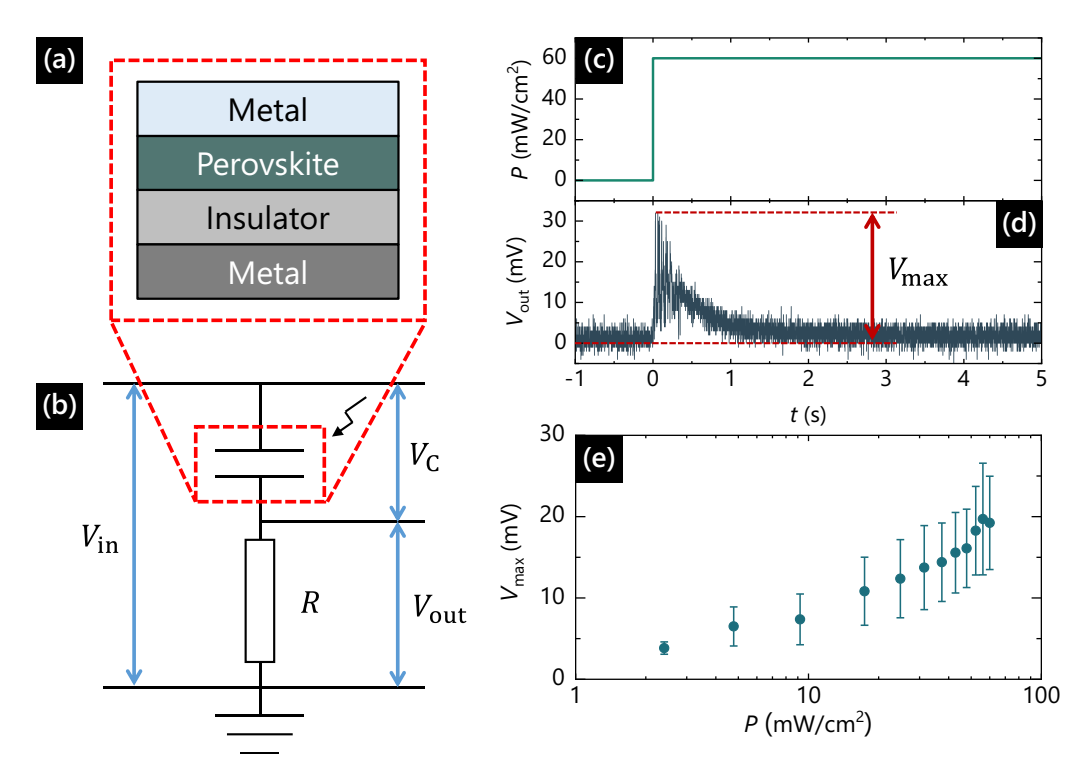


Figure 1. (a) Cross-sectional diagram of bilayer photosensitive capacitor employed in PRS (not to scale). The device is illuminated from above. (b) Circuit diagram of PRS formed of photosensitive bilayer capacitor and conventional resistor in series. (c) Optical power density, P, as a function of time, t, applied PRS. (d) Experimental output voltage of PRS, measured as a function of time. This sensor was identical to that described in our previous report: a highly doped silicon bottom electrode, 300 nm of thermally grown SiO₂ as the insulator, MAPbI₃ as the semiconductor, and 15 nm of gold as the top electrode. V_{max} denotes the approximate maximum voltage measured. (e) Experimentally measured V_{max} of 3 similar PRS as a function of optical power density. The error bars denote the standard deviation between values. $V_{\text{in}} = 5 \text{ V}$ in all cases. Reprinted with permission from [1]. Copyright (2020), AIP Publishing LLC.

[15], and for the top electrode we use 15 nm of either gold or aluminium. MAPbI₃ is known to be a strong absorber of light [11], and it changes conductance over many orders of magnitude under illumination [16]. The top electrode must be conducting, but also needs to allow optical access to the sample. While a thin layer of metal does provide the desired behaviour, it is here used out of convenience, and one would expect a much lower contact resistance if using a transparent conducting oxide (TCO) such as indium tin oxide (ITO) [17].

In our previous report [1], we used Kirchhoff's voltage law to derive a differential equation relating V_C to the timedependence of the capacitor, C. This equation is valid for any C(t), but needs to be solved numerically. This approach is valuable for demonstrating the anticipated response of PRS arrays to a complex time-varying visual field. However, when a simple input stimulus is used, such as that depicted in figure 1(c), it is possible to derive an approximate analytical relationship between V_{out} and P. We neglect the contact resistance of the top electrode R_C , in this analysis. We do so for two reasons. The first is that while a thin layer of Au or Al will give rise to a significant R_C [1], we anticipate most future device structures (such as those employing TCOs) will involve $R_C \ll R$. The second reason is conciseness. The incorporation of a finite R_C into this analysis is straightforward, however it adds little to the understanding of the device behaviour.

We describe the capacitance of the structure in figure 1(a) as follows:

$$C = C_{\rm D} + \alpha_0 P^{\gamma}. \tag{1}$$

 $C_{\rm D}$ is the capacitance of the structure in the dark, α_0 is the photo-capacitance prefactor and γ is a dimensionless exponent. This formulism is employed because most semiconductors are experimentally observed to obey a power law relationship between conductance and incident photon flux [18]. If we approximate charge carrier mobility to not be strongly dependent on incident photon density, then we can also assume that the charge density in the semiconductor, and hence the charge on the capacitor plates, Q, also obeys a power law. If $Q \propto P^{\gamma}$ for a constant voltage, which is what we would expect under constant illumination, then we can also reasonably conclude that $C \propto P^{\gamma}$.

Trap filling can occur in disordered semiconductors [19], which could conceivably reduce the activation energy under illumination in a system where charge transport is dominated by multiple trapping and release [20]. However, we anticipate this effect to be small relative to the generation of carriers. Furthermore, metal halide perovskites such as MAPbI₃ generally exhibit 'band-like' behaviour [21] when charges are studied by local techniques such as time resolved microwave conductivity [22] or optical-pump—THz probe spectroscopy [23]. This suggests that a temperature activated model is unlikely to be

appropriate for metal halide perovskites. For these reasons we neglect optically induced changes in carrier mobility.

We know from figure 1(b) that:

$$V_{\rm in} = V_C + V_{\rm out}. \tag{2}$$

Defining the current flowing in the circuit as I, we can use Ohm's law to say:

$$V_{\rm in} = V_C + IR. \tag{3}$$

Writing the current as the rate of change of charge (Q) through the circuit:

$$V_{\rm in} = V_C + R \frac{\mathrm{d}Q}{\mathrm{d}t}.\tag{4}$$

We identify the rate of change of charge as the rate of change of the product of capacitance and voltage:

$$V_{\rm in} = V_C + R \frac{\mathrm{d}}{\mathrm{d}t} \left[C V_C \right]. \tag{5}$$

In our device both C and V_C can vary as a function of time, so we must use the product rule to differentiate CV_C :

$$V_{\rm in} = V_C + R \left[C \frac{\mathrm{d}V_C}{\mathrm{d}t} + V_C \frac{\mathrm{d}C}{\mathrm{d}t} \right]. \tag{6}$$

We here restrict ourselves to optical stimuli which can be approximated as a step function, such as that depicted in figure 1(c). i.e. we describe C as follows:

$$C(t) = \begin{cases} C_{\rm D} & \text{if } t < 0 \\ C_{\rm D} + \alpha_0 P^{\gamma} & \text{if } t \geqslant 0 \end{cases}$$
 (7)

We can then approximate equation (6) as a difference equation across t=0. We say that a step change in capacitance, ΔC , will lead to a step change in voltage dropped across the capacitor, ΔV_C , over a period of time, Δt , where Δt is small:

$$V_{\rm in} = V_C + R \left[C \frac{\Delta V_C}{\Delta t} + V_C \frac{\Delta C}{\Delta t} \right]. \tag{8}$$

If the input voltage has been applied for a long period of time before the application of light, we assume that the input voltage will be dropped entirely across the capacitor in figure 1(b). Hence, we can say $V_C(t < 0) = V_{\rm in}$. We are interested in the peak value of $V_{\rm out}$ immediately after the light has been turned on, therefore we evaluate equation (8) at t=0, and we henceforth denote $V_C(t=0) \equiv V_C$ and $C(t=0) \equiv C$. Combined with equation (7), we can then express the differences in V_C and C as follows:

$$\Delta V_C = V_C - V_{\rm in} \tag{9a}$$

$$\Delta C = \alpha_0 P^{\gamma}. \tag{9b}$$

This then allows us to write equation (8) as follows:

$$V_{\rm in} = V_C + R \left[C \frac{V_C - V_{\rm in}}{\Delta t} + V_C \frac{\alpha_0 P^{\gamma}}{\Delta t} \right]. \tag{10}$$

Since the incident light intensity is assumed to go from 0 to P very quickly, we approximate $\Delta t \approx 0$. This leads to an expression for V_C :

$$V_C = V_{\rm in} \frac{C_{\rm D} + \alpha_0 P^{\gamma}}{C_{\rm D} + 2\alpha_0 P^{\gamma}}.$$
 (11)

Experimentally we measure V_{out} , not V_C . Using equation (2), and identifying $V_{\text{out}}(t=0) = V_{\text{max}}$, we can write equation (11) as follows:

$$V_{\text{max}} = V_{\text{in}} \left(\frac{\alpha_0 P^{\gamma}}{C_{\text{D}} + 2\alpha_0 P^{\gamma}} \right). \tag{12}$$

This equation can be fitted to the experimental V_{max} vs P data from figure 1(e), with α_0 and γ as fitting parameters. C_D was approximated to be 509 pF in our case, by considering the semiconductor and insulator as two capacitors in series. For this approximation the thickness of the semiconductor was set to 200 nm, the thickness of the insulator was 300 nm, the dielectric constant of the insulator was 3.9, the dielectric constant of the semiconductor was 20 [24], and the device area was 5 mm². This fit is shown in figure 2(a) for both devices studied. We see a broadly good agreement between experiment and theory. The extracted γ was 0.49 for the gold contact device and 0.37 for the aluminium contact device. Both are roughly consistent with previous values for MAPbI₃ evaluated using different techniques [18, 25]. The difference between the two values is possibly due to the low signal to noise and/or high contact resistance in the aluminium contact device. Because $C_{\rm D}$ was approximated here, rather than measured, we have not reported the other fitting parameter: α_0 . Capacitance measurements of metal halide perovskites are a rich and complex area of study [26], and one that is anticipated to be vitally important to understand these devices. Future studies of capacitance (in the dark and under illumination) will need to be a high priority for the PRS community in the future.

4. Peak output voltage

While equation (12) is useful, it can be rewritten in a more concise form if we define a new variable Λ as follows:

$$\Lambda = \frac{\alpha_0}{C_{\rm D}}.\tag{13}$$

From equation (12) we can then express the ratio of input to output voltages via equation (14):

$$\frac{V_{\rm in}}{V_{\rm max}} = 2 + \frac{1}{\Lambda P^{\gamma}}.\tag{14}$$

The value of γ will depend on the dominant recombination mechanism(s) in the semiconductor [27]. However, a special

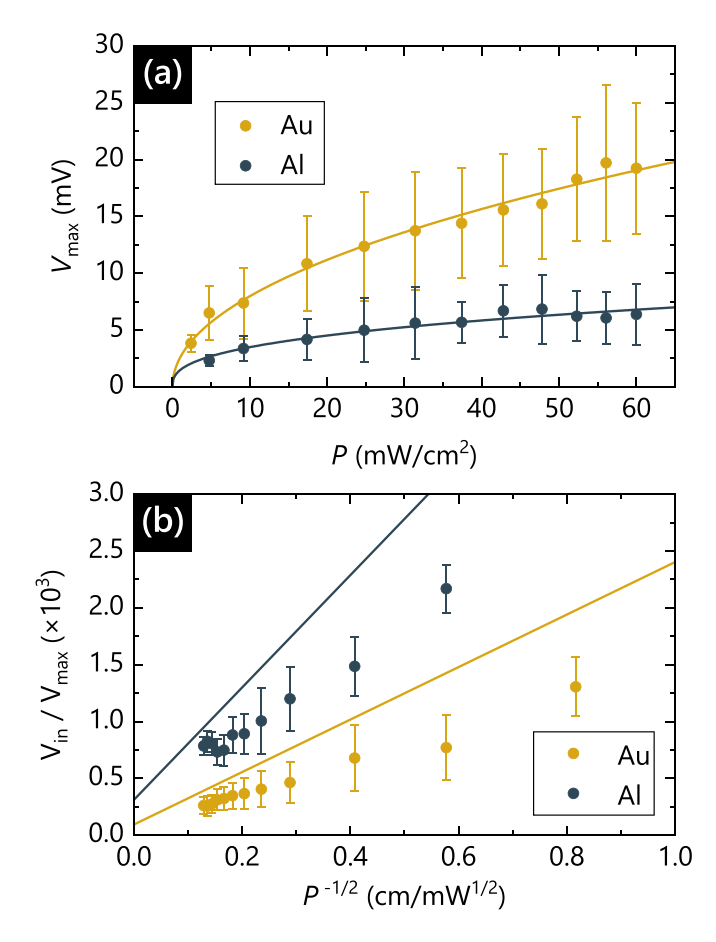


Figure 2. (a) Equation (12) fitted to experimentally measured $V_{\rm max}$, plotted as a function of optical power density (P) for PRSs. The fitted exponent was $\gamma=0.49$ for the gold (Au) top contact device and 0.37 for the aluminium (Al) contact device. (b) Equation (15) fitted to experimentally measured ratio of $V_{\rm in}/V_{\rm max}$, as a function of $P^{-1/2}$ for PRSs with gold (Au) and aluminium (Al) top contacts. Extracted Λ was 5.3×10^{-4} and 2.5×10^{-4} cm mW $^{-1/2}$ for gold and aluminium electrodes, respectively.

case exists when bimolecular recombination dominates and the density of holes and electrons are equal [18]. In this case $\gamma = 1/2$. If we approximate this to be true for all systems of interest to us, then we can rewrite equation (14) as:

$$\frac{V_{\rm in}}{V_{\rm max}} = 2 + \frac{1}{\Lambda P^{1/2}}.$$
 (15)

We acknowledge γ will not be $^{1}/_{2}$ for all semiconductors. However, there are significant benefits to making this approximation. The first is that we can now define the standard units of Λ to be cm mW $^{-1/2}$. If γ was different for every device, Λ would have different units for every device, making meaningful comparison impossible. Secondly, equation (15) now has only one fitting parameter: Λ , enabling unambiguous analysis. If the absorber does have a γ substantially different from 0.5, one would expect a non-linear relationship between $V_{\rm in}/V_{\rm max}$ and $P^{-1/2}$ to be observed experimentally. However, $V_{\rm max}/V_{\rm in}$ should still increase with Λ for a given range of P, meaning it can serve as a rough proxy for performance, nonetheless. Overall, making this assumption means a standard

Table 1. PRS figure of merit, Λ , for devices with gold (Au) and aluminium (Al) top electrode. Values were evaluated from the experimental data presented in figure 2(b) using equation (15). The value given is the mean between three identically prepared devices and the error is the standard deviation between these devices.

Electrode	$\Lambda ({\rm cm} {\rm mW}^{-1/2})$
Au	$5.3 \pm 1.2 \times 10^{-4}$
Al	$2.5 \pm 0.5 \times 10^{-4}$

experimental strategy to evaluate Λ can be formulated. This strategy is as follows:

- (a) Apply a constant $V_{\rm in}$ across the PRS.
- (b) Measure V_{out} as a function of time, in response to the application of light as a step function. Repeat this measurement for several values of P.
- (c) Extract the peak V_{out} , denoted V_{max} , for each P.
- (d) Plot $V_{\text{in}}/V_{\text{max}}$ on the y-axis against $P^{-1/2}$ on the x-axis.
- (e) A straight-line fit will yield a gradient of $1/\Lambda$.

We demonstrated this approach on two sets of experimental data, as shown in figure 2(b). The two sets of devices were identical except for the top electrode, which was gold in one case and aluminium in the other. The points shown are the mean of three devices, and the error bars are the standard deviation between the three devices. The range of measurements was larger using the Au electrode because $V_{\rm max}$ was too small to resolve at low P for the Al electrode devices. It is clear from figure 2(b) that carrying out measurements to as low a P as possible is desirable for an accurate fit. The extracted values of Λ for our two sets of devices are given in table 1. The lower Λ for the Al electrodes is attributed to higher optical absorption in the electrode than with Au. It is important to note that Λ is dependent upon the illumination wavelength, so the values in table 1 are only valid when the incident wavelength is 525 nm.

5. Performance limits

Since a PRS with a larger Λ will exhibit a larger $V_{\rm out}$, under identical illumination conditions, the parameter Λ represents a convenient metric to assess how responsive PRSs are to light. Λ also enables us to quantify both the maximum theoretical response, and a target practical response, of PRSs. From equation (15) we see that if Λ is finite, $V_{\rm max}/V_{\rm in} \to 0.5$ as $P \to \infty$. This means that the maximum peak output voltage for an PRS is half the input voltage. This is illustrated in figure 3(a), where $V_{\rm max}/V_{\rm in}$ is calculated as a function of P for various values of Λ . Because equation (15) states that a $V_{\rm max}/V_{\rm in}$ of 0.5 is impossible for finite optical power densities, we are forced to adopt a practical target $V_{\rm max}/V_{\rm in}$ below this. For the purposes of this report, we will choose a target practical limit of $V_{\rm max}/V_{\rm in}=0.4$ and base our subsequent discussion around this value.

For applications where bright sunlight is expected, we expect the maximum $V_{\rm max}/V_{\rm in}$ to be 0.4 when say $P=100~{\rm mW~cm^{-2}}$. For low light applications we define

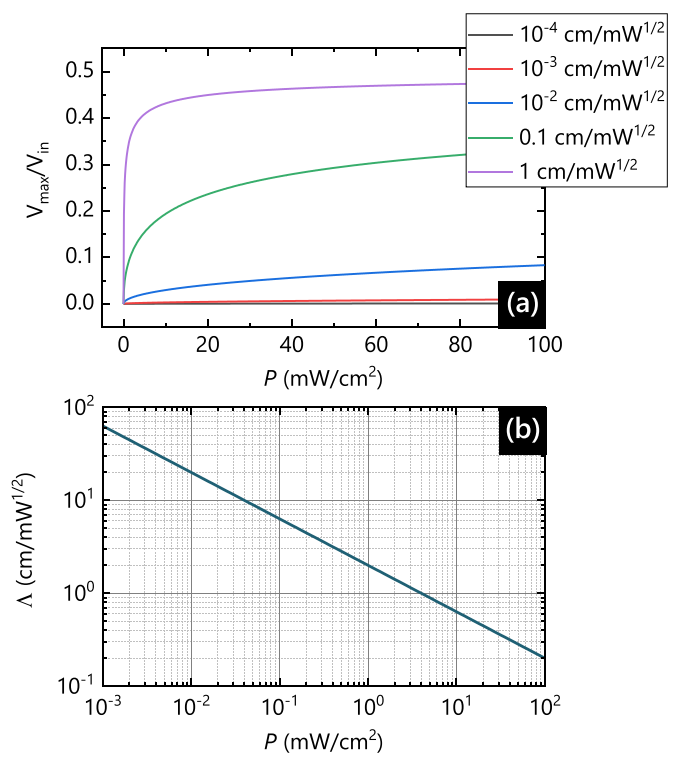


Figure 3. (a) Calculated ratio of $V_{\rm max}/V_{\rm in}$ as a function of input optical power density P, for PRSs with various values of Λ , using equation (15). (b) Calculated Λ to provide $V_{\rm max}/V_{\rm in}=0.4$, as a function of P, using equation (15).

the maximum $V_{\rm max}/V_{\rm in}=0.4$ when P=1 mW cm⁻² or lower. Figure 3(b) shows the required Λ for a device to exhibit $V_{\rm max}/V_{\rm in}=0.4$ as a function of P. While different requirements will exist for different conditions, it reasonable to conclude that PRSs with a $\Lambda \geqslant 1$ cm mW^{-1/2} would provide sufficient response under most normal situations. However, with an appropriate amplification strategy values below this are likely to be sufficient. For specialized applications with very low differences in light intensity (e.g. underwater, in space, or at night) $\Lambda \geqslant 10$ cm mW^{-1/2} would perhaps be a more appropriate target.

6. Factors affecting performance

6.1. Device area

From the definition of Λ in equation (13) it is clear that there are two main strategies to maximize the peak V_{out} in PRSs. The first is to increase the photo-capacitance prefactor α_0 , and the other is to reduce the dark capacitance C_{D} . Importantly, both α_0 and C_{D} are linearly proportional to the device area, A. This means that Λ and V_{max} are insensitive to area. Figure 4(a) shows calculated V_{out} as a function of t for a range of devices with different A, with otherwise identical parameters. This data was calculated by rewriting equation (6) in terms of V_{out} , and solving it numerically as a difference equation, in an analogous manner to our previous report [1].

Changing A will however change the device capacitance, which will in-turn affect the decay constant of the device τ ,

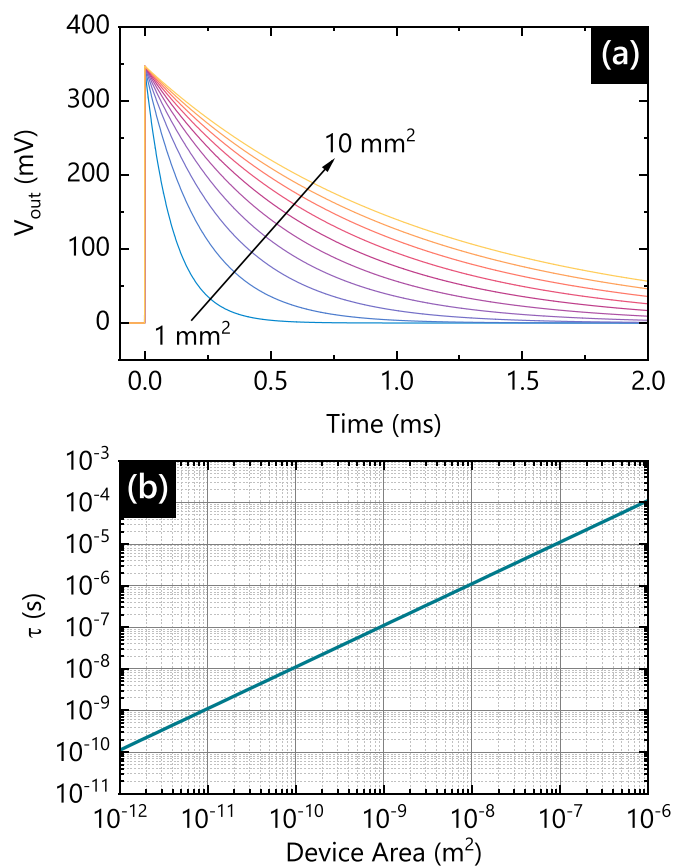


Figure 4. (a) Calculated $V_{\rm out}$ as a function of time, t, for ten different PRSs with a range of device areas, in response to a step-change in incident optical power density from 0 to 60 mW cm^{-2} at t=0. This data was calculated by solving equation (8) numerically as a difference equation. (b) Calculated decay time of PRSs as a function of device area, in response to a step-change in incident optical power density from 0 to 60 mW cm^{-2} . Besides device area and external resistance ($R=1 \text{ M}\Omega$), all other parameters were as observed experimentally for the Au-contact device.

through the RC constant. The voltage-time data plotted in figure 4(a) can be fitted to a monoexponential decay function to evaluate the time constant τ as a function of A. This is demonstrated as a function of device area in figure 4(b). Because it is normally straightforward to choose a value of R in figure 1(b) over a wide range of values, we can compensate for changes in A, by adjusting R. This means that neither peak height nor decay time of PRSs are limited by area.

6.2. Dark capacitance

The denominator in equation (13) is the capacitance in the dark: C_D . This means that Λ can be increased by decreasing the capacitance per unit area of the PRS in the dark. There are two strategies to decrease C_D : either decrease the relative permittivity of the semiconductor and/or insulator, or increase the thickness of these layers. Reducing the dielectric constant has limited scope because the minimum value of each layer is $\varepsilon_r = 1$. For example, if the devices studied in this report with gold electrodes had the semiconductor and insulator layers both replaced with materials where $\varepsilon_r = 1$, but were otherwise

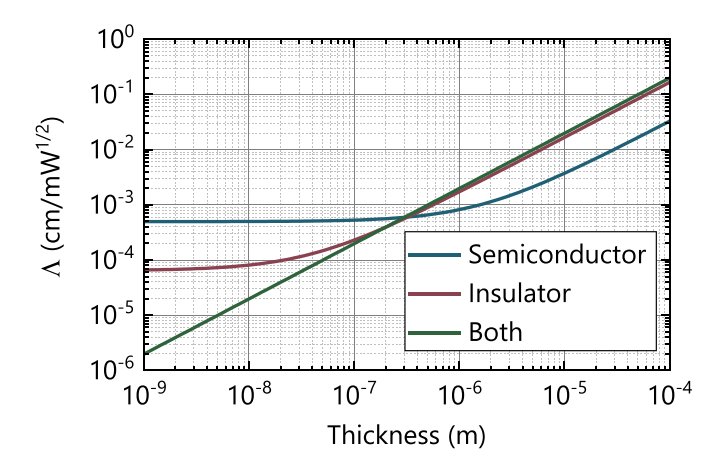


Figure 5. Calculated Λ as a function of the thickness of the semiconductor, insulator, or both. When not varied, the semiconductor thickness was set to 200 nm, and the insulator thickness was set to 300 nm. Besides layer thickness, all other parameters were as observed experimentally for the Au-contact device.

identical, the value of Λ would increase from 5.3 \times 10^{-4} to 3.1×10^{-3} cm mW $^{-1/2}$ only.

The other strategy to reduce C_D is to increase the thickness of the semiconductor and/or insulator. Because we model the semiconductor and insulator as capacitors in series, their capacitance is summed in reciprocal, meaning the layer with the largest thickness will dominate. For this reason, it is likely to be more practical to have a very thick layer of one material and a moderate/thin layer of the other. Increasing the thickness of the insulator may be technologically more convenient, especially if using a robust inorganic system such as SiO₂. However, increasing the thickness of the semiconductor has the added benefit of increasing the number of photons absorbed in the material, which would also increase α_0 . Figure 5 shows Λ calculated as a function of insulator thickness, semiconductor thickness, and both, where all other parameters (including α_0) are kept constant. We acknowledge that in reality increasing the semiconductor thickness will increase α_0 , especially for small thicknesses, but we here consider its effect on C_D only for the purposes of illustration. As an example, if we could increase the thickness of the SiO2 in our gold electrode devices from 300 nm to 3 μ m, while keeping all other parameters constant, Λ would increase from 5.3×10^{-4} to 4.8×10^{-3} cm mW^{-1/2}. Increasing C_D will also increase the decay time of the sensor, which would then need to be compensated for by reducing R.

6.3. Capacitance prefactor

The numerator in equation (13) is the photo-capacitance prefactor α_0 , hence increasing this parameter will increase Λ . α_0 will be higher for materials which yield a higher free charge density at the semiconductor–dielectric interface. To evaluate charge density under steady state illumination, one must equate generation and recombination. However, because the number of photons absorbed in the semiconductor will depend on depth into the material (via the Beer–Lambert law), the

charge generation rate will depend on position. This means that a full description must solve the carrier concentration as a function of position, accounting for diffusion due to charge density gradients, drift due to the externally applied field, and carrier injection and extraction across the semiconductormetal interface. Furthermore, holes and electrons are known to have dissimilar monomolecular lifetimes [28] (affecting recombination), charge carrier mobilities [21] (affecting diffusion and drift) and metal-band barrier heights [29] (affecting injection and extraction) in metal halide perovskites. The factors affecting α_0 are hence numerous and depend heavily on the semiconductor-metal combination employed. In the interest of brevity, we will not address these issues quantitatively here. We will, however, discuss some of the most important contributing factors to α_0 , qualitatively. Experimental measurements of capacitance as a function of illumination and voltage [26, 30, 31], combined with steady state photoconductance measurements [18, 25, 32] will likely be effective tools in understanding α_0 in the future.

It is clear that the optical absorbance of the semiconductor, and the transparency of the top electrode, are important. However, since TCOs have high optical transmittance [17], and metal halide perovskites have very high absorption coefficients [11], there is unlikely to be significant scope for optimization on these two parameters, especially since we in general want the semiconductor layers to be as thick as possible anyway. However, not all absorbed charges will lead to delocalized free carriers, as some will yield excitons which will recombine without affecting capacitance. This is quantified by the carrier generation yield ϕ , the number of free electronhole pairs generated per absorbed photon. This is a parameter which we would want to be as close to unity as possible in PRSs. Metal halide perovskites are known to have low exciton binding energies [33], making them good absorbers for this reason.

While crucially important in solar cells and transistors, charge carrier mobility is not as directly influential in PRS performance. Mobility will affect the drift and diffusion of carriers, which will in-turn affect the charge density at the interface between the semiconductor and dielectric. However, the nature of this relationship is complex. It will depend on the polarity of the applied voltage, the majority carrier type, the injection barrier between the semiconductor and metal, and the architecture employed. For example, if the semiconductor was illuminated from the side closest to the insulator (unlike the structure depicted in figure 1(a)) then a low mobility material may be desirable so charges drift and diffuse away from the semiconductor-dielectric interface more slowly.

Perhaps the most influential factor for α_0 is the average charge carrier lifetime. The carrier lifetime is conventionally quantified by rate constants associated with trap-assisted, bimolecular, and Auger processes: k_1 , k_2 , and k_3 respectively [34]. The relative contribution of k_1 , k_2 , and k_3 to average carrier lifetime depends on illumination intensity, with k_1 dominant for low P and k_2 , and k_3 dominant at higher P. Lower recombination rates would at first glance appear desirable in PRSs, as they will lead to a higher charge density under steady state conditions. However, long lifetimes will also result in

carrier densities changing over long period of time after illumination has been withdrawn or reduced. This would lead to a long decay time for $V_{\rm out}$ upon reducing light intensity, which may become relevant if a very high-speed response is required. For this reason, there may exist a fundamental tradeoff between τ and Λ in highly optimized PRSs.

7. Conclusions

In conclusion, we have presented a simple strategy to quantify the performance of PRSs. By measuring their peak output voltage in response to a discreet increase in illumination intensity, a broad proxy for performance, Λ , can be evaluated. A PRS with a larger Λ can be expected to yield a higher output voltage under identical illumination conditions. In its simplest description, this parameter should be independent of device area, illumination intensity, and magnitude of applied voltage. For this reason, it can be considered a useful metric to compare the response of retinomorphic sensors between different research groups, analogous to field effect mobility in transistors, or PCE in solar cells.

Using our model, we identified strategies to improve the performance of PRSs and defined approximate values that the community should consider targets for commercial viability. While here we only considered performance in response to a step function in light intensity, many of the considerations should be general. For example, the output voltage of a PRS in response to a constantly increasing optical power density should also scale with Λ .

From both an experimental and theoretical point of view, there remains much to be done on these sensors. In this report we focused on voltage response and did not explicitly consider the time scales involved in the device turning on or off, both of which are anticipated to be important for commercial applications. Similarly, we did not consider the behaviour due to changes between two non-zero power densities (e.g. movement in a bright setting), reductions in intensity, or optical stimuli besides step functions. Understanding the relationship between carrier density, illumination intensity, and voltage will also be critical for future optimization endeavours.

Data availability statement

The data that support the findings of this study are available upon reasonable request from the authors.

Acknowledgments

The authors thank the National Science Foundation for financial support (Award Number: 1942558). Part of this research was conducted at the Northwest Nanotechnology Infrastructure, a National Nanotechnology Coordinated Infrastructure site at Oregon State University which is supported in part by the National Science Foundation (Grant NNCI-2025489) and Oregon State University.

ORCID ID

John G Labram https://orcid.org/0000-0001-6562-9895

References

- [1] Trujillo Herrera C and Labram J G 2020 A perovskite retinomorphic sensor *Appl. Phys. Lett.* **117** 233501
- [2] Yu G, Srdanov G, Wang J, Wang H, Cao Y and Heeger A J 2000 Large area, full-color, digital image sensors made with semiconducting polymers Synth. Met. 111–2 133–7
- [3] Posch C, Serrano-Gotarredona T, Linares-Barranco B and Delbruck T 2014 Retinomorphic event-based vision sensors: bioinspired cameras with spiking output *Proc. IEEE* 102 1470–84
- [4] Lichtsteiner P, Posch C and Delbruck T 2008 A 128 \times 128 120 dB 15 μ s latency asynchronous temporal contrast vision sensor *IEEE J. Solid-State Circuits* 43 566–76
- [5] Brandli C, Berner R, Yang M, Liu S and Delbruck T 2014 A $240 \times 180 \ 130 \ dB \ 3 \ \mu s$ latency global shutter spatiotemporal vision sensor *IEEE J. Solid-State Circuits* 49 2333–41
- [6] Zaghloul K A and Boahen K 2006 A silicon retina that reproduces signals in the optic nerve J. Neural Eng. 3 257–67
- [7] Smeulders A W M, Chu D M, Cucchiara R, Calderara S, Dehghan A and Shah M 2014 Visual tracking: an experimental survey *IEEE Trans. Pattern Anal. Mach. Intell.* 36 1442–68
- [8] Fagnant D J and Kockelman K 2015 Preparing a nation for autonomous vehicles: opportunities, barriers and policy recommendations *Transp. Res.* 77 167–81
- [9] Almora O et al 2021 Device performance of emerging photovoltaic materials (version 1) Adv. Energy Mater. 11 2002774
- [10] Choi H H, Cho K, Frisbie C D, Sirringhaus H and Podzorov V 2017 Critical assessment of charge mobility extraction in FETs Nat. Mater. 17 2
- [11] de Wolf S, Holovsky J, Moon S-J, Löper P, Niesen B, Ledinsky M, Haug F-J, Yum J-H and Ballif C 2014 Organometallic halide perovskites: sharp optical absorption edge and its relation to photovoltaic performance *J. Phys. Chem. Lett.* 5 1035–9
- [12] Lee S-W et al 2016 UV degradation and recovery of perovskite solar cells Sci. Rep. 6 38150
- [13] Sze S M and Ng K K 2006 *Physics of Semiconductor Devices* (New York: Wiley)
- [14] Hong M J and Labram J G 2021 Inter-sample and intra-sample variability in electronic properties of methylammonium lead iodide Adv. Funct. Mater. 31 2101843
- [15] Snaith H J 2018 Present status and future prospects of perovskite photovoltaics *Nat. Mater.* 17 372–6
- [16] Perry E E, Labram J G, Venkatesan N R, Nakayama H and Chabinyc M L 2018 N-type surface doping of MAPbI₃ via charge transfer from small molecules *Adv. Electron. Mater.* 4 1800087
- [17] Kim H, Gilmore C M, Piqué A, Horwitz J S, Mattoussi H, Murata H, Kafafi Z H and Chrisey D B 1999 Electrical, optical, and structural properties of indium–tin–oxide thin films for organic light-emitting devices *J. Appl. Phys.* 86 6451–61
- [18] Levine I, Gupta S, Brenner T M, Azulay D, Millo O, Hodes G, Cahen D and Balberg I 2016 Mobility–lifetime products in MAPbI₃ films J. Phys. Chem. Lett. 7 5219–26
- [19] Olthof S, Mehraeen S, Mohapatra S K, Barlow S, Coropceanu V, Brédas J-L, Marder S R and Kahn A 2012 Ultralow doping in organic semiconductors: evidence of trap filling *Phys. Rev. Lett.* 109 176601

- [20] Mott S N F and Davis E A 1971 *Electronic Processes in Non-Crystalline Materials* (Oxford: Clarendon)
- [21] Herz L M 2017 Charge-carrier mobilities in metal halide perovskites: fundamental mechanisms and limits ACS Energy Lett. 2 1539–48
- [22] Oga H, Saeki A, Ogomi Y, Hayase S and Seki S 2014 Improved understanding of the electronic and energetic landscapes of perovskite solar cells: high local charge carrier mobility, reduced recombination, and extremely shallow traps J. Am. Chem. Soc. 136 13818–25
- [23] Milot R L, Eperon G E, Snaith H J, Johnston M B and Herz L M 2015 Temperature-dependent charge-carrier dynamics in CH₃NH₃PbI₃ perovskite thin films Adv. Funct. Mater. 25 6218–27
- [24] Wilson J N, Frost J M, Wallace S K and Walsh A 2019 Dielectric and ferroic properties of metal halide perovskites APL Mater. 7 010901
- [25] Labram J G, Perry E E, Venkatesan N R and Chabinyc M L 2018 Steady-state microwave conductivity reveals mobility-lifetime product in methylammonium lead iodide Appl. Phys. Lett. 113 153902
- [26] von Hauff E 2019 Impedance spectroscopy for emerging photovoltaics J. Phys. Chem. C 123 11329–46
- [27] Balberg I 1994 The two carriers' mobility-lifetime products and their light intensity dependencies in hydrogenated amorphous silicon J. Appl. Phys. 75 914–23

- [28] Hutter E M, Eperon G E, Stranks S D and Savenije T J 2015 Charge carriers in planar and meso-structured organic–inorganic perovskites: mobilities, lifetimes, and concentrations of trap states J. Phys. Chem. Lett. 6 3082–90
- [29] Schulz P, Cahen D and Kahn A 2019 Halide perovskites: is it all about the interfaces? Chem. Rev. 119 3349–417
- [30] Bou A, Pockett A, Raptis D, Watson T, Carnie M J and Bisquert J 2020 Beyond impedance spectroscopy of perovskite solar cells: insights from the spectral correlation of the electrooptical frequency techniques J. Phys. Chem. Lett. 11 8654–9
- [31] Hailegnaw B, Sariciftci N S and Scharber M C 2020 Impedance spectroscopy of perovskite solar cells: studying the dynamics of charge carriers before and after continuous operation *Phys. Status Solidi* a 217 2000291
- [32] Watts C L, Aspitarte L, Lin Y-H, Li W, Elzein R, Addou R, Hong M J, Herman G S, Snaith H J and Labram J G 2020 Light soaking in metal halide perovskites studied via steady-state microwave conductivity *Commun. Phys.* 3 1–10
- [33] Miyata A, Mitioglu A, Plochocka P, Portugall O, Wang J T-W, Stranks S D, Snaith H J and Nicholas R J 2015 Direct measurement of the exciton binding energy and effective masses for charge carriers in organic-inorganic tri-halide perovskites *Nat. Phys.* 11 582–7
- [34] Herz L M 2016 Charge-carrier dynamics in organic-inorganic metal halide perovskites Annu. Rev. Phys. Chem. 67 65–89